



AMERICAN METEOROLOGICAL SOCIETY

Weather and Forecasting

EARLY ONLINE RELEASE

This is a preliminary PDF of the author-produced manuscript that has been peer-reviewed and accepted for publication. Since it is being posted so soon after acceptance, it has not yet been copyedited, formatted, or processed by AMS Publications. This preliminary version of the manuscript may be downloaded, distributed, and cited, but please be aware that there will be visual differences and possibly some content differences between this version and the final published version.

The DOI for this manuscript is doi: 10.1175/WAF-D-16-0182.1

The final published version of this manuscript will replace the preliminary version at the above DOI once it is available.

If you would like to cite this EOR in a separate work, please use the following full citation:

Dong, J., R. Domingues, G. Goni, G. Halliwell, H. Kim, S. Lee, M. Mehari, F. Bringas, J. Morell, and L. Pomales, 2017: Impact of assimilating underwater glider data on Hurricane Gonzalo (2014) forecast. *Wea. Forecasting*. doi:10.1175/WAF-D-16-0182.1, in press.



1
2 **Impact of assimilating underwater glider data**
3 **on Hurricane Gonzalo (2014) forecast**
4

5
6 Jili Dong^{1,2*}, Ricardo Domingues^{3,4}, Gustavo Goni⁴, George Halliwell⁴, Hyun-Sook
7 Kim^{1,2}, Sang-Ki Lee⁴, Michael Mehari^{3,4}, Francis Bringas⁴, Julio Morell⁵, Luis Pomales⁵
8

9
10 ¹I.M. System Group, Inc., Rockville, MD, USA

11 ²National Oceanic and Atmospheric Administration, Environmental Modeling Center,
12 Marine Modeling and Analysis Branch, College Park, MD, USA

13 ³University of Miami, Cooperative Institute for Marine and Atmospheric Studies, Miami,
14 FL, USA

15 ⁴National Oceanic and Atmospheric Administration, Atlantic Oceanographic and
16 Meteorological Laboratory, Physical Oceanography Division, Miami, FL, USA

17 ⁵University of Puerto Rico Mayaguez, Department of Marine Sciences, Mayaguez,
18 Puerto Rico
19

20 **Submitted to Weather and Forecasting October 2016**

21 **Revised February 2017**
22
23

* Corresponding author address: Dr. Jili Dong, NOAA/NCWCP, 5830 University
Research Ct., College Park, MD 20740, E-mail: jili.dong@noaa.gov

24 **Abstract**

25 The initialization of ocean conditions is essential to coupled tropical cyclone (TC)
26 forecasts. This study investigates the impact of ocean observations assimilation,
27 particularly underwater glider data, on high-resolution coupled TC forecasts. Using the
28 coupled Hurricane Weather Research and Forecasting (HWRF) - Hybrid Coordinate
29 Ocean Model (HYCOM) system, numerical experiments are performed by assimilating
30 underwater glider observations alone and with other standard ocean observations for the
31 forecast of Hurricane Gonzalo (2014). The glider observations are able to provide
32 valuable information on sub-surface ocean thermal and saline structure, even with their
33 limited spatial coverage along the storm track and relatively small amount of data
34 assimilated. Through the assimilation of underwater glider observations, the pre-storm
35 thermal and saline structures of initial upper ocean conditions are significantly improved
36 near the location of glider observations, though the impact is localized due to the limited
37 coverage of glider data. The ocean initial conditions are best represented when both the
38 standard ocean observations and the underwater glider data are assimilated together. The
39 barrier layer and the associated sharp density gradient in the upper ocean are successfully
40 represented in the ocean initial conditions only with the use of underwater glider
41 observations. The upper ocean temperature and salinity forecasts in the first 48 hours are
42 improved by assimilating both underwater glider and standard ocean observations. The
43 assimilation of glider observations alone does not make large impact on the intensity
44 forecast due to their limited coverage along the storm track. The 126-hour intensity

45 forecast of Hurricane Gonzalo is improved moderately through assimilating both
46 underwater glider data and standard ocean observations.

47

48

49 **1. Introduction**

50 Interaction between the upper-ocean and tropical cyclones (TCs) may partly drive
51 further intensification or dissipation through several key feedback mechanisms such as
52 the development of turbulent mixing, upwelling, and baroclinic adjustment processes
53 (e.g., Price et al. 1994; Dickey et al. 1998; Prasad and Hogan 2007). While baroclinic
54 adjustment processes (i.e. propagation of inertial-internal waves in the thermocline)
55 provide one way of dispersing the energy introduced by hurricane winds in the ocean
56 (Shay and Elsberry 1987; Brink 1989), turbulent mixing and upwelling may also lead to
57 upper-ocean cooling, which is often linked to hurricane intensity changes and possibly
58 dissipation (e.g., Glenn et al. 2016). The upper ocean response and related air-sea
59 interface variability are critical for TC development (Cione 2015).

60 Turbulent mixing is the main process leading to upper ocean cooling, while
61 hurricane forced upwelling can also contribute to the cooling. The latter is manifested
62 significantly for a slow-moving storm, in general less than $\sim 4 \text{ ms}^{-1}$ (Price 1981; Prasad
63 and Hogan 2007; Yablonsky and Ginis 2009; Halliwell et al. 2015). Nevertheless, there
64 are occasions when specific characteristics of ocean conditions can suppress turbulent
65 mixing and sea surface cooling. For example, the presence of barrier layers (Balaguru et
66 al. 2012a; Grodsky et al. 2012; Domingues et al. 2015), and/or large upper ocean heat
67 content (Shay et al. 2000; Lin et al. 2008; Mainelli et al. 2008; Goni et al. 2015) can
68 efficiently reduce storm-induced SST cooling. Barrier layers are usually linked with low
69 salinity waters near the surface, associated with the heavy precipitation that accompanies
70 a storm or freshwater discharge from the Amazon and Orinoco rivers (e.g. Kelly et al.

71 2000; Corredor et al. 2003; Balaguru et al. 2012a; Johns et al. 2014). The low salinity
72 values near the surface define strong stratification conditions that often exceed the effects
73 of vertical shear (e.g., Domingues et al. 2015), and physically suppress turbulent mixing
74 and SST cooling. When the effects of vertical shear exceed the influence of stratification,
75 strong hurricane-forced SST cooling may sometimes be observed (Glenn et al. 2016).

76 Hurricane-forced upper-ocean cooling may subsequently lead to a reduction in the
77 intensity of the storm by limiting air-sea fluxes of heat and moisture. This negative
78 feedback mechanism is more effective for slower moving storms (Halliwell et al. 2015),
79 and for storms that travel over areas with low upper-ocean heat content, often referred as
80 Tropical Cyclone Heat Potential (TCHP) (Goni et al. 2009). TCHP is defined as the
81 thermal energy required to increase temperature above 26 °C, integrated from the ocean
82 surface to the depth of the 26⁰C isotherm. TCHP is considered a key factor affecting air-
83 sea interaction in tropical cyclone forecasts (Mainelli et al. 2008; Goni et al. 2009; Lin et
84 al. 2012). Areas with high TCHP and deep mixed layers require very strong turbulent
85 shear to entrain sufficient thermocline waters to cool the mixed layer. In these areas,
86 higher TCHP favor hurricane intensification by suppressing SST cooling underneath the
87 storm, and maintaining the surface sensible and latent heat fluxes from the ocean to the
88 atmosphere (Lin et al. 2008; Mainelli et al. 2008). In fact, ocean observations and
89 analysis showed that Hurricane Opal (1995) (Shay et al. 2000) and Hurricane Katrina
90 (Mainelli et al. 2008) experienced rapid intensification (defined as a 30 kt increase in
91 wind speed within 24 hours) while travelling over anticyclonic features with high TCHP
92 in the Gulf of Mexico.

93 Therefore, in order to improve hurricane intensity forecasts within a coupled
94 atmosphere-ocean model, it is critical to provide ocean initial conditions that accurately
95 represent the ocean thermal and saline structures (Chan et al. 2001; Emanuel et al. 2004;
96 Wang and Wu 2004; Halliwell et al. 2015), particularly in the upper ocean. Underwater
97 gliders (gliders hereafter) are an excellent observational platform for providing a large
98 number of ocean profile observations with a rather flexible navigation and sampling
99 strategy that can be adapted according to the projected storm track (Domingues et al.
100 2015). Gliders can be piloted along predetermined tracks and configured at any time to
101 update the navigation and other relevant parameters, such as the spatial and temporal
102 sampling strategy. Gliders can also effectively provide sustained and targeted ocean
103 observations under hurricane force wind conditions, offering a cost-effective
104 observational platform to complement other observations, such as Argo floats and
105 Airborne Expendable BathyThermograph (AXBT). Many efforts have been made in
106 recent years to assimilate glider data in regional or coastal ocean models to improve
107 ocean initialization (Oke et al. 2009; Shulman et al. 2009; Dobricic et al 2010; Zhang et
108 al. 2010; Pan et al. 2011; Yaremchuk et al. 2011; Jones et al 2012; Melet et al. 2012;
109 Gangopadhyay et al. 2013; Mourre and Chiggiato 2014; Pan et al. 2014). Rudnick (2016)
110 summarized some of the above data assimilation studies in a review paper. All of the
111 studies demonstrated the positive impact of assimilating glider data on ocean forecasts.

112 This study focuses on the impact of assimilating glider observations on ocean
113 initialization and hurricane prediction within the Hurricane Weather Research and
114 Forecast (HWRF)-HYbrid Coordinate Ocean model (HYCOM) coupled hurricane

115 forecast system. This is the first study of its kind to investigate the impact of ocean
116 observations on hurricane forecasting in this region using a convection-permitting
117 atmosphere-ocean coupled hurricane model.

118 The case study presented in this manuscript focuses on Hurricane Gonzalo
119 (2014), the strongest hurricane in the North Atlantic Ocean from 2011 to 2014. TC
120 Gonzalo started to develop as a tropical storm in the tropical North Atlantic Ocean on
121 October 12, 2014. The storm travelled to the west and developed into a Category 1
122 hurricane on October 13 2014. Gonzalo rapidly intensified to a Category 3 hurricane on
123 October 14, and continued to intensify to a Category 4 hurricane on October 15 with
124 maximum sustained winds of 115 kts (Brown 2015). Before Gonzalo started to recurve
125 northeastward on October 16, it experienced an eyewall replacement cycle and slightly
126 weakened (Fig. 1) (Brown 2015). Gonzalo reached its peak intensity of 125 kts at 1200
127 UTC October 16. After that stage, increasing wind shear and cooler sea surface
128 temperature (SST) weakened Gonzalo while it continued to accelerate north-
129 northeastward (Brown 2015). The 126-hour coupled model simulation analyzed in this
130 manuscript covers the rapid intensification of Gonzalo and its subsequent life cycle from
131 October 13 to October 18.

132 This manuscript is organized as follows: pre-storm upper ocean conditions before
133 the passage of Gonzalo are discussed in section 2. Section 3 describes the coupled model,
134 data assimilation system, experiment setup, and ocean observations. The impacts of
135 glider observations on ocean initial conditions and subsequent ocean and hurricane

136 forecasts are examined in sections 4 and 5, respectively. Section 6 provides a summary of
137 this study.

138

139 **2. Upper ocean conditions during Hurricane Gonzalo (2014)**

140 Two gliders were deployed in mid-July 2014 to sample the ocean conditions
141 during the Atlantic hurricane season of 2014. One glider was deployed in the Caribbean
142 Sea (not shown) and the other in the tropical North Atlantic (Fig. 2a). Both gliders were
143 piloted along predetermined fixed tracks, obtaining approximately 12 temperature and
144 salinity profiles per day between the surface and 1000 m depth. Temperature and salinity
145 (T/S) profiles collected by the two gliders in October 2014 provided key profile
146 observations of the upper ocean structures before, during, and after the passage of
147 Gonzalo. These data were assimilated into the HYCOM ocean model to assess the impact
148 of glider data on HWRF-HYCOM forecasting skill.

149 During October 8-13, 2014, the glider traveled along section AB, sampling pre-
150 storm temperature and salinity conditions between the surface and 1000 m depth. From
151 October 13 to 15, the glider was parked at the location B to measure the ocean response
152 during the passage of the storm. During its intensification to Category 3, the center of
153 Hurricane Gonzalo was positioned at 20.8°N, 65.6°W, approximately 85 km northeast of
154 glider location B, north of Puerto Rico (Fig. 2a). Pre-storm temperature observations
155 showed that there was an upper layer with homogenous temperature of ~29°C above 50
156 m (Fig. 2b), and that the depth of the 26°C isotherm was located at about 90 m depth
157 along the section A-B. It is estimated here that the TCHP in the region along section AB

158 was approximately 86 kJ cm^{-2} , well above the 50 kJ cm^{-2} threshold for sustaining a
159 hurricane in the tropical North Atlantic Ocean (Mainelli et al. 2008). Salinity
160 observations (Fig. 2c) showed that, north of 20.6°N , a homogenous salinity layer with
161 values of 36.7 psu was observed above 90 m. South of this latitude, a shallow low-
162 salinity layer was observed above 20 m, with values as low as 35.8 psu at site B (Fig. 2e).
163 The observed reduction in salinity leads to a strong density stratification above 50 m
164 (Domingues et al. 2015; Fig. 7 of this study).

165 Satellite-derived observations for October 13, 2014, indicate that warm surface
166 waters with SST larger than 28.5°C (Fig. 8a) extended through a large area around the
167 location of the glider, and that Hurricane Gonzalo traveled most of the time over areas
168 that had initial SSTs larger than 26°C (Fig. 8a). While most areas along the track of
169 Gonzalo were initially associated with SSTs above 26°C , satellite-derived TCHP
170 indicates that values above 60 kJ cm^{-2} were mostly found south of 25°N (Fig. 8e), in
171 agreement with the glider observations (section 4.1). Larger hurricane-induced upper
172 ocean cooling is therefore expected north of this latitude (Lin et al. 2008).

173 Upper-ocean heat content observed along the track of hurricane Gonzalo on
174 October 2014 was anomalously high with respect to the historical record (Fig. 3). The
175 space (latitude) - time diagram of sea height residuals (SHR, annual cycle removed)
176 along section AB (Fig. 3a) shows that the signal is dominated by positive values of SHR
177 starting in 2012. Positive SHRs are of special interest because they indicate warm
178 monthly anomalies with respect to the upper-ocean heat content since 1993. In October
179 2014, SHRs reached values of 10 cm above the long-term average for October during the

180 1993-2015 period, suggesting that upper ocean conditions were warmer than usual in this
181 location. Analysis of TCHP residuals at site B during 1993-2015 (Fig. 3b) further
182 indicates that the upper-ocean heat content on October 2014 was $\sim 15 \text{ kJ cm}^{-2}$ higher than
183 the average conditions observed in this area.

184 The analysis above shows that ocean conditions in October 2014 were favorable
185 overall for the development and potential intensification of Hurricane Gonzalo (2014).
186 The presence of larger than average upper-ocean heat content and of a 20 m thick barrier
187 layer along the track of Gonzalo may have largely suppressed the hurricane-forced SST
188 cooling. This cooling ranged between -0.4°C and -1°C in the region sampled by the glider
189 (Domingues et al. 2015), and peaked at -2°C when Hurricane Gonzalo reached maximum
190 intensity as a category 4 hurricane at 23.5°N – 68.0°W (Goni et al. 2015). The small
191 upper-ocean cooling caused by the hurricane may have favored further intensification.

192

193 **3. Model and data assimilation experiment setup**

194

195 **3.1 The HWRF-HYCOM coupled model**

196

197 The coupled model used in this study is the HWRF-HYCOM system, consisting
198 of the atmospheric model HWRF and the ocean model HYCOM. The HWRF model is
199 the operational numerical model for hurricane forecasting used by the Environmental
200 Modeling Center (EMC) of the National Centers for Environmental Prediction (NCEP),
201 and provides real-time tropical cyclone prediction during hurricane seasons. This model
202 has three domains (27-9-3 km horizontal resolutions) with the two nesting domains

203 moving with a storm. HWRF solves the governing non-hydrostatic equations on the
204 rotated longitude-latitude horizontal mesh and 63 hybrid pressure-sigma vertical layers
205 extending up to 2 hPa. The physical parameterizations used in HWRF include cumulus
206 convection in the intermediate and outer domains, Ferrier microphysics, modified Global
207 Forecast System (GFS) planetary boundary layer (PBL), Rapid Radiative Transfer Model
208 for General circulation models (RRTMG) long- and short-wave radiation, and HWRF
209 surface flux (Soloviev et al. 2014). The details of physical parameterizations can be
210 found in the HWRF science document (Tallapragada et al. 2015).

211 The ocean model HYCOM has a single domain with a uniform horizontal
212 resolution of $1/12^\circ$ to cover the North Atlantic. This model has 32 hybrid vertical levels
213 that include the terrain-following coordinate near the coast, the z coordinate in the mixed
214 layers, and the isopycnal coordinate in deep water. The vertical mixing process is
215 parameterized with the K-profile parameterization scheme (KPP). In the coupling system,
216 HYCOM receives the wind stress, surface sensible and latent heat flux, net longwave and
217 shortwave radiation and precipitation from HWRF, while HYCOM feeds the SST to the
218 HWRF model at every 540 s coupling time.

219

220 3.2 Experiment setup and observations

221 The atmospheric component model was initialized using the GFS analysis at 0000
222 UTC on October 13, 2014. The initial storm was first relocated to the location of the
223 National Hurricane Center best track. The vortex intensity and size are adjusted
224 according to the storm message file or TC vitals, using the HWRF vortex initialization
225 package. The initialization details can also be found in the HWRF scientific document

226 (Tallapragada et al. 2015). The lateral boundary conditions of HWRP used in this work
227 were derived from the GFS forecast. No atmospheric data assimilation was performed in
228 this study.

229 The ocean initial conditions were obtained from the ocean forecast-data assimilation
230 cycle system maintained at the Physical Oceanography Division (PHOD) of the Atlantic
231 Oceanographic and Meteorological Laboratory (AOML), of the National Oceanic and
232 Atmospheric Administration (NOAA). The ocean data assimilation system used in this
233 study employed a statistical interpolation method, where users can specify
234 forecast/background error covariance flexibly (Halliwell et al. 2014). In this study, an
235 ensemble of model states sampled at different times was used to represent the forecast
236 error covariance (Halliwell et al. 2014).

237 Additional ocean observations assimilated, other than those obtained by the gliders,
238 include along-track measurements of sea surface height anomaly (SSHA) from three
239 satellite altimeters (Jason-1, Jason-2 and Envisat), SST from the satellite-derived
240 multichannel SST (MCSST) product, in-situ measurements collected by ships, surface
241 buoys and surface drifters, temperature profile data from expendable bathythermographs
242 (XBT), and Argo floats. An example of the distribution of these standard ocean
243 observations distribution from different ocean observing platforms (from September 29 to
244 October 13 2014) is plotted in Fig. 4. The observation errors specified in the data
245 assimilation system for each of the above types are the same as in Halliwell et al. (2014).
246 All observations mentioned above are denoted as standard observations, as compared to
247 glider observations. The localization or cutoff radii for each data type are also consistent

248 with Table 3 of Halliwell et al. (2014). All standard observations were assimilated daily
249 from 0000 UTC March 1 of 2014 throughout 0000 UTC October 13 2014. For the
250 underwater glider T/S profiles, the observation error is 0.01 °C for temperature and 0.02
251 psu for salinity. Among the T/S profile data from two gliders, only observations at 0000
252 UTC were assimilated from 0000 UTC July 15 to 0000 UTC October 13, 2014. The
253 numbers of each observation type assimilated in this study are listed in Table 1.

254 In this study, an unconstrained ocean simulation from September 2008 through 2014,
255 denoted as NODA, was used as the benchmark experiment. Three data assimilation
256 experiments were designed to examine the impact of assimilating underwater glider T/S
257 data and standard observations, and they are denoted as GLID (assimilation of glider data
258 only), CTRL (assimilation of all ocean data except glider data) and ALL (assimilation of
259 all ocean data) (Table 2). After the initialization of both atmospheric and ocean models,
260 the 126-hour coupled hurricane forecast is run from 0000 UTC October 13 until 0600
261 UTC October 18, covering most of the life cycle of Gonzalo as the category of hurricane.

262

263 **4. Impact of underwater gliders on initial ocean conditions**

264 **4.1 Impact of underwater glider observations on upper ocean temperature and** 265 **salinity structure**

266 The pre-storm upper ocean thermal and saline structures directly affect the ocean
267 response to hurricanes and the related SST cooling (Emanuel et al. 2004; Yablonsky and
268 Ginis 2009; Halliwell et al. 2015). The pre-storm ocean conditions were sampled by the
269 underwater glider while it was located at 66° W, 20.2° N at 0000 UTC on October 13,
270 about 781 km away from the eye of Gonzalo (59.7° W 16.5° N). To examine the impact

271 of assimilating underwater glider T/S data and other standard ocean observations on the
272 pre-storm upper ocean conditions, the initial T/S conditions from four experiments at
273 0000 UTC on October 13 were interpolated to the glider location and compared to the
274 glider T/S profiles (Fig. 5), used here as the ground truth. The differences between model
275 outputs and the glider observation (model - obs) were calculated (Fig. 6).

276 The pre-storm ocean profile exhibited a mixed layer around 55 m deep and an
277 SST of 29⁰C (black line in Fig. 5a). The temperature profile of NODA showed a much
278 shallower mixed layer depth of 10 m deep and negative bias across the upper 150 m of
279 the ocean. The model SST was 0.2⁰C colder than the glider observation, with the surface
280 layer temperature showing a local maximum bias of -1.5⁰C at the observed mixed layer
281 base of 55 m (Fig. 6a). The negative temperature bias continued to increase from 65 m to
282 the deeper ocean and reached values beyond -1.5⁰C below 100 m. The assimilation of
283 glider T/S profiles in GLID improved the vertical thermal structure by reducing the bias
284 throughout most of the upper 150 m (Fig. 6b). The SST of GLID was warmer than the
285 observed by only 0.3⁰C, and the local maximum of surface layer temperature error was
286 found at the mixed layer base, 0.9⁰C smaller than that of NODA. The bias was always
287 below 0.4⁰C between 60 and 120 m and increased to 1⁰C down to 150 m. The
288 temperature profile of CTRL is similar to GLID above the mixed layer base (55 m) and
289 had a bias always higher than 0.5⁰C from 60 m to 150 m (Fig. 6c), which suggests that
290 the assimilation of other standard observations also improved the pre-storm thermal
291 structure, although not as much as assimilating the glider T/S profiles. The assimilation
292 of glider data together with other standard observations further improved the initialization

293 of the ocean thermal structure around the glider location, as the mixed layer depth of
294 ALL was around 30 m, deeper than CTRL but still 25 m shallower than observed (Fig.
295 6d). The shallower mixed layer of the model simulations was partly due to the deficiency
296 of the vertical mixing scheme and/or the data assimilation system, such as the static
297 background covariance structure. The temperature bias in ALL was further reduced over
298 most of the upper 150 m compared to CTRL. There was a 0.3°C degradation at 55 m of
299 ALL over CTRL, which was probably caused by inaccurate background/forecast error
300 covariance.

301 The TCHP estimated from glider observations at around 66° W, 20.2° N was
302 approximately 86 kJ cm⁻². The TCHP values calculated from four experiments at the
303 glider location were 59, 81, 92 and 81 kJ cm⁻² for NODA, GLID, CTRL and ALL,
304 respectively. The assimilation of glider observations greatly reduced the TCHP
305 underestimate from 27 in NODA to 5 kJ cm⁻² in GLID, reducing the percentage
306 underestimate from 31% to 6%. Given that the threshold of TCHP for maintaining TC
307 development is around 50 kJ cm⁻² (Mainelli et al. 2008), an error reduction of 22 kJ cm⁻²
308 is notable, and may translate into significant changes in the intensity forecast of
309 Hurricane Gonzalo. While CTRL over-estimated the TCHP by 6 kJ cm⁻², the additional
310 assimilation of glider data led to a TCHP under-estimation by 5 kJ cm⁻² in ALL.

311 The saline structure is a key factor to determine the density field, and therefore
312 influences vertical mixing that may affect TC intensification (Balaguru et al. 2012b;
313 Domingues et al. 2015). The observed subsurface salinity quickly increased from the
314 surface to 36.5 psu at 20 m (Fig. 5b). NODA underestimated the salinity with negative

315 bias over 0.5 psu from 20 m down to 150 m depth (Fig. 6e). The assimilation of glider
316 T/S data in either GLID or ALL greatly reduced the negative bias down to 0.2 psu (Fig.
317 6f and h). Assimilating the other standard observations also helped to reduce the error,
318 although not as much as the assimilation of glider observations (Fig. 6g). The salinity of
319 ALL was very close to the observations between 20 and 105 m with near-zero errors (Fig.
320 6h).

321 Accurate representation of upper level density change, barrier layer and ocean
322 stratification is essential to potentially improve the air-sea interaction and ocean feedback
323 in the model, and in turn the TC forecast. The observed rapid salinity reduction from the
324 surface to 20 m depth led to a sharp gradient of density over the shallow upper layers (Fig.
325 7a), forming a 20 m thick barrier layer. The barrier layer, caused by the upper layer
326 salinity change, tends to resist vertical mixing and thus has the potential to reduce TC-
327 forced SST cooling (Wang et al. 2011; Balaguru et al. 2012b). Balaguru et al. (2012b)
328 showed that barrier layers can significantly influence TC intensification by modifying the
329 SST cooling and air-sea heat flux exchange. This important feature of the density change
330 and barrier layer was not well retrieved when ocean data was not assimilated (NODA).
331 Assimilating other standard observations resulted in little improvement, with the density
332 profile still smoothly increasing over the upper 50 m in both NODA and CTRL. On the
333 other hand, with glider data assimilated in GLID and ALL (Fig. 7a and b), the sharp
334 vertical density gradient was better retrieved in the upper 20 m and the density profile of
335 GLID over the upper 35 m was reasonably close to the observations (Fig. 7a). The
336 improvement in the representation of the barrier layer and ocean stratification was also

337 evident in assessing the buoyancy frequency N^2 (Fig. 7b). Large positive N^2 , defined as
338 Brunt-Vaisala frequency, represents strong stability. The observations showed strong
339 stability and stratification in the upper 20 m, which was better represented by the
340 assimilation of glider data (GLID and ALL). The buoyancy frequency of GLID and ALL
341 was almost twice that of NODA and CTRL. The barrier layer in GLID and ALL was
342 about 20 m thick, and did not exist in NODA and CTRL.

343 In summary, the assimilation of underwater glider data improved ocean
344 initialization by reducing the error of pre-storm, upper thermal and saline structures and
345 producing a deeper isothermal layer and larger TCHP. The largest error reduction was
346 mostly found below the mixed layer. One important result of the study, and applicable to
347 this experiment only, is that the improvement from assimilating other standard
348 observations is significant, however it is not as large as that obtained from assimilating
349 glider T/S data alone. Assimilating both standard and glider observations (ALL) appears
350 to have the largest improvement on upper ocean initial conditions. Assimilation of glider
351 data also improved the model representation of the upper-ocean density structure that
352 included a barrier layer, which was accurately represented only when glider data was
353 assimilated.

354 4.2 The impact of underwater glider observations on pre-storm SST and TCHP

356 The impact of assimilating glider observations is not only limited to the exact
357 location of the observations. The error covariance and local radii combined determine
358 how far the impact of observations will reach by the assimilation. Further forecast cycles
359 will spread the impact of data assimilation even beyond the time and location of the
360

361 assimilation. In this section, the initial large-scale ocean environment along the path of
362 Gonzalo is briefly examined to assess how far and how large the impact of ocean data
363 assimilation may reach. The values of SST and TCHP in the vicinity of the path of
364 Gonzalo are of particular interest here.

365 Fig. 8 shows initial SST conditions for the three experiments at 0000 UTC
366 October 13 2014 overlapped with the 126-hour predicted track of each storm. The best
367 track is superimposed on the Remote Sensing Systems (RSS) SST fields retrieved from
368 satellite microwave and IR products and optimally interpolated (OI) at 9 km resolution
369 (Fig. 8a). The pre-storm ocean conditions show a large body of warm water region with
370 SSTs over 28.5°C in the Caribbean Sea and southern region of the North Atlantic
371 subtropical gyre, which is known as Atlantic Warm Pool and closely correlated with
372 Atlantic hurricane activity (e.g., Wang and Lee 2007). Hurricane Gonzalo crossed over
373 this warm pool region that exhibited SSTs above 29°C before and in the vicinity of the
374 hurricane track recurvature, coinciding with the rapid intensification of the storm. When
375 no observations were assimilated, the warm pool in NODA is weaker and smaller
376 compared to the satellite derived values. SSTs never exceeded 29°C around and along
377 the storm track (Fig. 8b). The assimilation of glider data greatly helped to improve the
378 warm pool around both glider locations and over the storm path (Fig. 8c). With standard
379 observations assimilated in CTRL, the warm pool structure is much better retrieved in a
380 larger area. The warm pool structure of the environment and along the storm path is close
381 to those in observations in terms of both strength and coverage (Fig. 8d). The additional

382 impact of the assimilation of glider data in ALL was relatively minor (not shown), due to
383 the limited space covered by the glider observations.

384 The results presented above are also illustrated in Fig. 9. The initial SST along the
385 projected 126-hour path of each storm (0000 UTC October 13 to 0600 UTC October 18)
386 is averaged within a radius of 84 km from storm centers (~ 2 radii of maximum wind
387 R_{\max}) (Fig. 9). From 6 to 90 hours, the observed initial SST remained around 29°C , while
388 NODA never reached 29°C along the storm path. When the glider data were assimilated,
389 the averaged along-storm SST in GLID was largely corrected to the observed value in the
390 region close to the glider location (dashed line). The largest reduction of SST error along
391 the track forecast is around 0.7°C over NODA. The averaged initial SST value in CTRL
392 follows the observations quite well from 18 to 96 hours with a 0.4°C overestimation
393 around 48 hours on the projected storm path. This 0.4°C positive bias is corrected by
394 assimilating the glider data in ALL.

395 The initial TCHPs from the model are also shown in Fig. 8 and compared to the
396 TCHP field produced at AOML/PHOD. The latter product is calculated from the
397 altimeter-derived vertical temperature profiles estimates in the upper ocean (Dong et al.
398 2015). The impact of assimilating glider observations data on the TCHP distribution is
399 consistent with the conclusion on SST: GLID improves over NODA while TCHP of
400 CTRL is better initialized within a much larger area (Fig. 8e-h).

401

402

403 **5. Impact of underwater glider data on the coupled forecast**

404

405 **5.1 Impact on ocean forecast**

406

407 The ocean component of the coupled forecast system provides the necessary
408 oceanic feedback to the hurricane. Correctly predicting the ocean processes under strong
409 hurricane wind conditions is critical to improve the parameterization of air-sea interaction
410 and hurricane forecast. As shown in section 4.1, the pre-storm ocean temperature and
411 salinity (T/S) conditions were improved by the assimilation of underwater glider
412 observations. We examined here whether the improvements will be maintained in the
413 subsequent unconstrained ocean forecast by comparing the ocean forecasts with glider
414 observations collected during the passage of Hurricane Gonzalo.

415 The observed ocean response to Hurricane Gonzalo obtained from the underwater
416 glider data was discussed in Domingues et al. (2015). During 0000 UTC October 13 to
417 0000 UTC October 15, the underwater glider was parked at 66° W, 20.2° N (site B),
418 providing a good opportunity to measure the in-storm ocean response. In this section, we
419 mostly focus on the forecast error evolution of the four data (or no data) assimilation
420 experiments during the 48-hour period. The forecast error is defined here as the
421 difference between the forecast and the glider data (model minus observation). The
422 temperature and salinity error evolution of the upper 150 m depth is shown in Fig. 10 and
423 Fig. 11, respectively.

424 Temperature errors in NODA are always negative with values above 0.6 °C
425 throughout the whole upper 150 m depth. The error changes only little in the two-day
426 forecast (Fig. 10a). NODA also underestimates salinity (Fig. 11a) by at least 0.5 psu
427 during most of the 48 forecast hours below 15 m depth. The assimilation of glider data
428 significantly improves the initial T/S structure and also the subsequent ocean forecasts

429 (Fig. 10b): forecast temperature error is clearly reduced above 30 m and the absolute
430 error value is below 0.2 °C during most of two-day forecast in GLID. Below 60 m depth,
431 the errors are also reduced. From 0800 UTC October 13 to 2000 UTC October 14, the
432 temperature error below 100 m in GLID is mostly under 0.4 °C. The salinity forecast in
433 GLID also generates a smaller error than NODA mostly below 30 m depth (Fig. 11b).
434 The magnitude of the salinity error largely remains below 0.3 psu. The assimilation of
435 other standard ocean observations (CTRL) also helps to improve the ocean forecast (Fig.
436 10c and Fig. 11c). Temperature errors are greatly reduced above 40 m depth. Below the
437 mixed layer, forecasts from CTRL have error always being positive in 48-hour forecast in
438 the upper thermocline (Fig. 11c). Similar to GLID, the salinity forecast in CTRL shows
439 error reduction below 40 m depth, while the error between 40 and 100 m is generally
440 smaller than in GLID (Fig. 11c). The additional assimilation of glider data in ALL further
441 reduces both the temperature and salinity errors over CTRL (Fig. 10d and Fig. 11d). For
442 temperature, the forecast error below 60 m is clearly reduced throughout the upper 150 m
443 depth during most of the time for the two-day forecast, and the error in the upper 30 m is
444 slightly smaller than in CTRL (Fig. 10d). For salinity, the negative bias of CTRL in the
445 upper 40 m is greatly reduced (Fig. 11d). The salinity error between 100 m to 150 m
446 depth also decreases, with the resulting error throughout the whole 150 m depth always
447 below 0.3 psu during most of 48-hour forecasts.

448 In general, the ocean forecast errors of temperature and salinity during the first 48
449 hours are reduced by either the assimilation of glider data alone or by additional
450 assimilation using other standard ocean observations when verified against the glider T/S

451 observations. Among the four experiments examined in this study, the assimilation of
452 both the standard ocean observations and underwater glider data (e.g. all ocean
453 observations available) produces the best ocean temperature and salinity forecast in terms
454 of error reduction.

455 456 **5.2 Impact on Hurricane Gonzalo's forecast**

457 We showed in section 4 that the assimilation of glider T/S data improves the upper
458
459 ocean thermal and saline conditions in areas that were directly under or in the proximity
460 of the track of Hurricane Gonzalo. In this section, we will discuss the impact of initial
461 ocean condition improvements on Hurricane Gonzalo forecasts in the coupled forecast
462 system. To accomplish this, the track and intensity forecasts of Hurricane Gonzalo from
463 different experiments will be examined.

464 The track forecasts of Gonzalo from the four experiments are shown in Fig. 12a,
465 along with the observed best track. Gonzalo first moved to the northwest and along the
466 southwest edge of North Atlantic subtropical gyre. After staying over the warm waters of
467 the Antilles current, Gonzalo started to recurve slowly towards the northeast at 1200 UTC
468 October 16. It continued to move northeast and weakened along the path until 0600 UTC
469 October 18. The predicted tracks follow the best track closely except for the last 36 hours
470 of the period when all the predicted storms move slower than the best track. Most of the
471 predicted tracks exhibit a southward displacement during the first 54 hours and an
472 eastward bias by forecast hour 90. Tropical storm translation speed is crucial for
473 controlling the underlying ocean response and the subsequent SST cooling feedback to
474 the storm (Lin et al. 2009; Mei et al. 2012; Halliwell et al. 2015). The average 126 hours

475 translation speeds of the four experiments are 5.0, 5.1, 4.7 and 4.9 m s⁻¹ respectively,
476 slightly slower compared to 5.4 m s⁻¹ of the best track and statistically equivalent, all
477 indicating intermediate translation speeds (between 4 and 6 m s⁻¹; Mei et al. 2012). The
478 difference among the track forecasts from the four experiments is relatively small,
479 suggesting the ocean data assimilation has little impact on the track forecast and/or a
480 relatively high predictability of track forecasts in this particular case. Since TC track
481 forecast is largely dependent on steering flow (Chan 2005; Chan 2009), the small track
482 spread among the experiments suggests that the large-scale atmospheric circulation is not
483 significantly altered by the underlying ocean in the relatively short forecast period (126
484 hours) for this particular case. The initial atmospheric conditions are identical in all four
485 experiments, and they all use the same GFS boundary conditions.

486 In order to assess the intensity forecasts, the 126-hour minimum sea level pressure
487 and maximum surface wind forecasts of Gonzalo are evaluated (Fig. 12b and c). The
488 actual storm intensified quickly in the first 60 hours from a tropical storm with a center
489 pressure of 1002 hPa and maximum surface wind of 40 knots at 0000 UTC October 13
490 (59.7° W, 16.5° N), to a category 3 major hurricane with 949 hPa center pressure and 115
491 knots wind at 1200 UTC October 15 (67.7° W, 23.2° N). Gonzalo continued to intensify
492 in the next 24 hours to a category 4 hurricane with a 940 hPa center pressure and 125
493 knots wind at 1200 UTC October 16 (68.7° W, 25.6° N), which was also the strongest
494 stage of the life cycle of this storm.

495 When there are no ocean observations assimilated (NODA), the forecast model fails
496 to predict the rapid intensification of Gonzalo (Figures 12b and 12c). The predicted storm

497 slowly intensified and the forecasted center pressure and surface maximum wind are
498 always weaker than the best track after 30 hours. The strongest storm peak predicted in
499 NODA has a center pressure of 957 hPa and maximum surface wind of 90 knots, which
500 is only a category 2 hurricane. The assimilation of the data from the underwater gliders in
501 GLID has little impact on the intensity forecast with small differences of both the center
502 pressure and maximum wind between NODA and GLID. The intensity forecast is
503 considerably improved by the assimilation of other standard ocean observations in CTRL.
504 CTRL predicts a rapid intensification of Gonzalo with the predicted center pressure of
505 Gonzalo up to 13 hPa deeper than the best track during 12 to 48 hours. The center
506 pressure of CTRL after 0000 UTC October 15 is much closer to that from the best track
507 and the largest difference is more than 15 hPa stronger than NODA. The peak intensity of
508 CTRL reaches to 943 hPa and 103 knots, putting it to a category 3 hurricane. The
509 additional assimilation of underwater glider in ALL shows a slight improvement over
510 CTRL. The intensity of ALL further deepens to 939 hPa and 107 knots, with larger
511 improvement over CTRL for the maximum wind during 78 to 108 hours forecasts than
512 other forecast hours. This result suggests that assimilating glider data, if added to the
513 existing observations, makes a larger impact on the intensity forecast of Hurricane
514 Gonzalo than assimilating glider data alone. The limited coverage of glider observations,
515 and relatively small amount of glider observations assimilated along the storm track,
516 make the impact of assimilating glider observations much less significant than the impact
517 of assimilating standard ocean observations.

518 It is also noticed that the predicted maximum surface wind from the coupled model
519 forecasts always falls below the observations with a negative bias, although the central
520 pressure is more or less comparable to the best track. This inconsistency is observed
521 when the model overestimates the storm size so that a storm with the same center
522 pressure but a larger size will produce smaller pressure gradients and weaker winds.
523 Studies on how to improve TC size prediction are still ongoing and a better understanding
524 of the physical processes related to TC intensification will help to improve the forecasts.

525

526 **6. Conclusions**

527 This study aims to investigate the impact of underwater glider observations
528 assimilation on hurricane forecasts using a high resolution coupled atmospheric-ocean
529 numerical model system. Within this context, the ocean initialization and data
530 assimilation are critical to providing an accurate ocean status for the coupled forecast.
531 The hypothesis of this work is that underwater gliders provide a flexible sampling
532 strategy and have the potential to improve hurricane forecasts by representing a more
533 accurate ocean structure for the coupled system. Hurricane Gonzalo (2014) was selected
534 as the study case, because the ocean conditions were favorable for hurricane
535 intensification.

536 The pre-storm ocean thermal conditions on 2014 October are first compared with
537 those of previous years. This comparison shows that the pre-storm upper ocean
538 temperatures during October 2014 were higher than average and, thus, had the potential
539 for TC development and intensification.

540 Results obtained here for this particular case study show that when the T/S data
541 extracted from underwater gliders are assimilated either alone or together with standard
542 ocean observations, the pre-storm ocean thermal and saline structures are significantly
543 improved. The improvement on pre-storm ocean SST is not limited to the exact location
544 of the glider but also extends to areas surrounding the observation. It is also observed that
545 the mixed layer depth, although improved by the assimilation of glider data, is still
546 shallower than the observations. This is probably caused by simplified assumptions and
547 inaccurate horizontal and vertical covariance of the statistical interpolation approach.
548 More advanced data assimilation methods, e.g. variational or ensemble-based data
549 assimilation may help to alleviate the problem.

550 The improvement in the initial saline structure from the assimilation of underwater
551 glider data leads to better initialization of ocean density structures. The sharp density
552 gradient and the related barrier layer are well represented only when underwater glider
553 observations are assimilated. This improvement on the barrier layer and density structure
554 proves the importance of glider data assimilation in initializing ocean conditions.

555 Our analysis shows that the assimilation of the standard ocean observations
556 improves the intensity forecast of Gonzalo, having smaller errors in minimum center
557 pressure and maximum surface wind. However, the assimilation of underwater glider
558 observations alone does not have a significant impact on the intensity forecast. As
559 Halliwell et al. (2015) demonstrated with very idealized one dimensional ocean coupling
560 forecast experiments, storms with intermediate translation speeds are less sensitive to the
561 changes in TCHP than slow moving storms (their Fig. 4). Furthermore, their study has

562 shown the TC response to change of ocean thermal structure is gradual: for small storms
563 moving at an intermediate speed, it may take 12 hours for the adjustment to become
564 completely substantial after the storm eye passes the cool/hot ocean boundary. The above
565 study suggests that change of storm intensity is highly dependent on the horizontal scale
566 of ocean features along the storm track: the storm has to stay over a particular ocean
567 feature long enough (e.g. more than 12 hours) to be effectively influenced. In our case
568 study with Gonzalo, which is a relatively small storm with intermediate translation speed,
569 the impact of assimilating glider observations may still be too localized along the storm
570 track to affect the storm intensity significantly (Fig. 9). On the other hand, the other
571 standard ocean observations, especially satellite altimeter observations, cover a large area
572 over the full storm track (Fig. 4) and produce a significant improvement of the intensity
573 forecast. Additional glider observations, if deployed along the storm tracks, may be able
574 to help to improve the ocean conditions covering a larger area and thus affect the
575 intensity more efficiently.

576 The ocean forecasts produced by the coupled system are improved from assimilating
577 glider observations by largely reducing both temperature and salinity forecast errors near
578 the glider location. The assimilation of both standard and glider observations produces
579 the best ocean forecast and characterization, when compared against with the glider T/S
580 observations. Results presented here indicate that for this case study the combination of
581 glider data and standard ocean observations leads to the best hurricane intensity and
582 ocean forecast, highlighting the impact of assimilating surface and profile ocean
583 observations to improve the coupled hurricane intensity forecast.

584 Our investigation of ocean data assimilation on hurricane forecasts has shown
585 promising results as the key step into this challenging topic. More TC cases will be
586 examined to obtain a rigorous conclusion on the role of ocean observations with different
587 sampling strategies for the coupled TC forecast.

588 Compared to other standard ocean observations, the innovative glider observations
589 still have a limited spatial coverage and the amount of observations available is relatively
590 small so far, as shown in Table 1. Larger impact of glider assimilation was observed
591 when combined with the standard ocean observations in this particular case.
592 Notwithstanding the limited spatial coverage of glider observations, assimilation of glider
593 data is still able to provide valuable information on sub-surface thermal and saline
594 structures of the ocean for coupled TC forecasts that is vital for model evaluation and
595 improvement efforts. A similar procedure in the project supporting this study will be
596 performed to extend the glider network: once the areas where hurricanes have historically
597 intensified are identified, a well-designed glider network will be deployed. The collected
598 data will then be assimilated to drive the coupled forecast for selected TC cases, and their
599 impact will be evaluated. Such approach will be first tested within an observing system
600 simulation experiments (OSSE) framework. A glider network of 12-18 gliders will be
601 simulated and assimilated for multiple TC cases within the OSSE framework and their
602 impact will be assessed. Future studies will also examine the individual impact of
603 temperature and salinity profile data from gliders on ocean initialization and TC forecast.
604 A more advanced data assimilation system, e.g. utilizing variational or ensemble-based

605 data assimilation techniques, is also expected to help further maximize the ocean
606 observations' impact.

607

608

609 **Acknowledgements:**

610 The authors would like to thank Dr. Frank Marks, Dr. Libby Johns and three anonymous
611 reviewers for their constructive and very helpful comments to this manuscript. This work
612 was supported by the Disaster Relief Appropriations Act of 2013 (P.L. 113-2), also
613 known as the Sandy Supplemental, through the NOAA research grant
614 NA14OAR4830103, by NOAA's Atlantic Oceanographic and Meteorological Laboratory,
615 and by CariCOOS (Caribbean Coastal Observing System).

616

617 **References**

618

619 Balaguru, K., P. Chang, R. Saravanan, and C. J. Jang, 2012a: The Barrier Layer of the

620 Atlantic warm pool: Formation mechanism and influence on the mean climate. *Tellus*

621 *A*, **64**.

622 Balaguru, K., P. Chang, R. Saravanan, L. R. Leung, Z. Xu, M. Li, and J.-S. Hsieh, 2012b:

623 Ocean barrier layers' effect on tropical cyclone intensification. *Proceedings of the*

624 *National Academy of Sciences*, **109**, 14343-14347.

625 Brink, K. H., 1989: Observations of the Response of Thermocline Currents to a

626 Hurricane. *J. Phys. Oceanogr*, **19**, 1017-1022.

627 Brown, D. P., 2015: National Hurricane Center Tropical Cyclone Report: Hurricane

628 Gonzalo (AL082014).

629 Chan, J. C. L., 2005: The physics of tropical cyclone motion. *Annual Review of Fluid*

630 *Mechanics*, Annual Reviews, 99-128.

631 Chan, J. C. L., 2009: Movement of Tropical Cyclones. *Global Perspectives on Tropical*

632 *Cyclones – From Science to Mitigation*, J. C. L. Chan, and J. Kepert, Eds., World

633 Scientific, 133-148.

634 Chan, J. C. L., Y. Duan, and L. K. Shay, 2001: Tropical Cyclone Intensity Change from a

635 Simple Ocean–Atmosphere Coupled Model. *J. Atmos. Sci.*, **58**, 154-172.

636 Cione, J., 2015: The relative roles of the ocean and atmosphere as revealed by buoy air-

637 sea observations in hurricanes. *Mon. Wea. Rev.*, **143**, 904-913.

638 Corredor, J., J. Morell, J. López, R. Armstrong, A. Dieppa, C. Cabanillas, A. Cabrera,

639 and V. Hensley, 2003: Remote continental forcing of phytoplankton biogeochemistry:

640 Observations across the “Caribbean-Atlantic front”. *Geophys. Res. Lett.*, **30**, 2057,
641 doi:10.1029/2003GL018193,20.

642 Dickey, T., D. Frye, J. McNeil, D. Manov, N. Nelson, D. Sigurdson, H. Jannasch, D.
643 Siegel, T. Michaels, and R. Johnson, 1998: Upper-Ocean Temperature Response to
644 Hurricane Felix as Measured by the Bermuda Testbed Mooring. *Mon. Wea. Rev.*, **126**,
645 1195-1201.

646 Dobricic, S., N. Pinardi, P. Testor, and U. Send, 2010: Impact of data assimilation of
647 glider observations in the Ionian Sea (Eastern Mediterranean). *Dynamics of*
648 *Atmospheres and Oceans*, Volume 50, Issue 1, 78-92,
649 doi:10.1016/j.dynatmoce.2010.01.001.

650 Dong, S ., G. Goni , and F. Bringas, 2015: Temporal variability of the Meridional
651 Overturning Circulation in the South Atlantic between 20S and 35S. *Geophys. Res.*
652 *Lett.*, **42**, 7655 - 7662, doi:10.1002/2015GL065603.

653 Domingues, R., G. Goni, F. Bringas, S.-K. Lee, H.-S. Kim, G. Halliwell, J. Dong, J.
654 Morell, and L. Pomales, 2015: Upper ocean response to Hurricane Gonzalo (2014):
655 Salinity effects revealed by targeted and sustained underwater glider observations.
656 *Geophys. Res. Lett.*, **42**, 7131-7138.

657 Emanuel, K., C. DesAutels, C. Holloway, and R. Korty, 2004: Environmental Control of
658 Tropical Cyclone Intensity. *J. Atmos. Sci.*, **61**, 843-858.

659 Gangopadhyay, A., A. Schmidt, L. Agel, O. Schofield, and J. Clark, 2013: Multiscale
660 forecasting in the western North Atlantic: Sensitivity of model forecast skill to glider

661 data assimilation. *Continental Shelf Research*, Volume 63, Supplement, S159-S176,
662 doi:10.1016/j.csr.2012.09.013.

663 Glenn, S. M., T. N. Miles, G. N. Seroka, Y. Xu, R. K. Forney, F. Yu, H. Roarty, O.
664 Schofield, and J. Kohut, 2016: Stratified coastal ocean interactions with tropical
665 cyclones. *Nat Commun*, **7**.

666 Goni, G., J. A. Knaff, and I.-I. Lin, 2015: [The Tropics] Tropical cyclone heat potential,
667 [in "State of the Climate in 2014"]. *Bull. Amer. Meteor. Soc.* **96**, S121-S122.

668 Goni, G., M. DeMaria, J. Knaff, C. Sampson, I. Ginis, F. B. A. Mavume, C. Lauer, I.-I.
669 Lin, M. M. Ali, P. Sandery, S. Ramos-Buarque, K. Kang, A. Mehra, E. Chassignet,
670 and G. Halliwell, 2009: Applications of satellite-derived ocean measurements to
671 tropical cyclone intensity forecasting. *Oceanography*, **22**, 190-197.

672 Grodsky, S. A., N. Reul, G. Lagerloef, G. Reverdin, J. A. Carton, B. Chapron, Y. Quilfen,
673 V. N. Kudryavtsev, and H.-Y. Kao, 2012: Haline hurricane wake in the
674 Amazon/Orinoco plume: AQUARIUS/SACD and SMOS observations. *Geophys. Res.*
675 *Lett.*, **39**, L20603, doi:10.1029/2012GL053335.

676 Halliwell, G. R., S. Gopalakrishnan, F. Marks, and D. Willey, 2015: Idealized Study of
677 Ocean Impacts on Tropical Cyclone Intensity Forecasts. *Mon. Wea. Rev.*, **143**, 1142-
678 1165.

679 Halliwell, G. R., A. Srinivasan, V. Kourafalou, H. Yang, D. Willey, M. L. Hénaff, and R.
680 Atlas, 2014: Rigorous Evaluation of a Fraternal Twin Ocean OSSE System for the
681 Open Gulf of Mexico. *J. Atmos. Oceanic Technol.*, **31**, 105-130.

682 Johns, E. M., B. A. Muhling, R. C. Perez, F. E. Müller-Karger, N. Melo, R. H. Smith, J.
683 T. Lamkin, T. L. Gerard, and E. Malca, 2014: Amazon River water in the
684 northeastern Caribbean Sea and its effect on larval reef fish assemblages during April
685 2009. *Fisheries Oceanography*, **23**, 472-494.

686 Jones, E. M., P. R. Oke, F. Rizwi, and L. M. Murray, 2012: Assimilation of glider and
687 mooring data into a coastal ocean model. *Ocean Modelling*, Volume 47, 1-13,
688 doi:10.1016/j.ocemod.2011.12.009.

689 Kelly, P. S., K. M. M. Lwiza, R. K. Cowen, and G. J. Goni, 2000: Low-salinity pools at
690 Barbados, West Indies: Their origin, frequency, and variability. *J. Geophys. Res.:*
691 *Oceans*, **105**, 19699-19708.

692 Lin, I.-I., C.-C. Wu, I.-F. Pun, and D.-S. Ko, 2008: Upper-Ocean Thermal Structure and
693 the Western North Pacific Category 5 Typhoons. Part I: Ocean Features and the
694 Category 5 Typhoons' Intensification. *Mon. Wea. Rev.*, 136, 3288-3306.

695 Lin, I.-I., I.-F. Pun, and C.-C. Wu, 2009: Upper-Ocean Thermal Structure and the
696 Western North Pacific Category 5 Typhoons. Part II: Dependence on Translation
697 Speed. *Mon. Wea. Rev.*, **137**, 3744-3757.

698 Lin, I.-I., G. J. Goni, J. A. Knaff, C. Forbes, and M. M. Ali, 2012: Ocean heat content for
699 tropical cyclone intensity forecasting and its impact on storm surge. *Natural Hazards*,
700 **66**, 1481-1500.

701 Mainelli, M., M. DeMaria, L. K. Shay, and G. Goni, 2008: Application of Oceanic Heat
702 Content Estimation to Operational Forecasting of Recent Atlantic Category 5
703 Hurricanes. *Wea. Forecasting*, **23**, 3-16.

704 Mei, W., C. Pasquero, and F. Primeau, 2012: The effect of translation speed upon the
705 intensity of tropical cyclones over the tropical ocean. *Geophys. Res. Lett.*, **39**,
706 L07801, doi:10.1029/2011GL050765.

707 Melet, A., J. Verron, and J. M. Brankart, 2012: Potential outcomes of glider data
708 assimilation in the Solomon Sea: Control of the water mass properties and parameter
709 estimation, *Journal of Marine Systems*, Volume 94, 232-246,
710 doi:10.1016/j.jmarsys.2011.12.003.

711 Mourre, B., and J. Chiggiato, 2014: A comparison of the performance of the 3-D super-
712 ensemble and an ensemble Kalman filter for short-range regional ocean prediction.
713 *Tellus A*, [S.l.], doi:10.3402/tellusa.v66.21640.

714 Oke, P. R., P. Sakov, and E. Schulz, 2009: A comparison of shelf observation platforms
715 for assimilation in an eddy-resolving ocean model, *Dynamics of Atmospheres and*
716 *Oceans*, Volume 48, Issues 1–3, 121-142, doi:10.1016/j.dynatmoce.2009.04.002.

717 Pan, C., M. Yaremchuk, and D. Nechaev, 2011: Variational assimilation of glider data in
718 the Monterey Bay. *Journal of Marine Research*, 69 (2-3), 331-346.

719 Pan, C., L. Zheng, R. H. Weisberg, Y. Liu, and C. E. Lembke, 2014: Comparisons of
720 different ensemble schemes for glider data Assimilation on West Florida Shelf.
721 *Ocean Modelling*, 81, 13-24.
722

723 Prasad, T. G., and P. J. Hogan, 2007: Upper-ocean response to Hurricane Ivan in a 1/25°
724 nested Gulf of Mexico HYCOM. *J. Geophys. Res.: Oceans*, **112**, C04013.

725 Price, J. F., 1981: Upper Ocean Response to a Hurricane. *J. Phys. Oceanogr*, **11**, 153-
726 175.

727 Price, J. F., T. B. Sanford, and G. Z. Forristall, 1994: Forced Stage Response to a Moving
728 Hurricane. *J. Phys. Oceanogr.*, **24**, 233-260.

729 Rudnick, D. L., 2016: Ocean research enabled by underwater gliders. *Annu. Rev. Mar.*
730 *Sci.*, **8**, 519–541, doi:10.1146/annurev-marine-122414-033913.

731 Shay, L. K., and R. L. Elsberry, 1987: Near-Inertial Ocean Current Response to
732 Hurricane Frederic. *J. Phys. Oceanogr.*, **17**, 1249-1269.

733 Shay, L. K., G. J. Goni, and P. G. Black, 2000: Effects of a Warm Oceanic Feature on
734 Hurricane Opal. *Mon. Wea. Rev.*, **128**, 1366-1383.

735 Shulman, I., C. Rowley, S. Anderson, S. DeRada, J. Kindle, P. Martin, J. Doyle, J.
736 Cummings, S. Ramp, F. Chavez, D. Fratantoni, and R. Davis, 2009: Impact of glider
737 data assimilation on the Monterey Bay model. *Deep Sea Research Part II: Topical*
738 *Studies in Oceanography*, Volume 56, Issues 3–5, 188-198,
739 doi:10.1016/j.dsr2.2008.08.003.

740 Soloviev, A. V., R. Lukas, M. A. Donelan, B. K. Haus, and I. Ginis, 2014: The air-sea
741 interface and surface stress under tropical cyclones. *Scientific Reports*, **4**, 5306.

742 Tallapragada, V., L. Bernardet, M. K. Biswas, I. Ginis, Y. Kwon, Q. Liu, T. Marchok, D.
743 Sheinin, B. Thomas, M. Tong, S. Trahan, W. Wang, R. Yablonsky, and X. Zhang,
744 2015: *Hurricane Weather Research and Forecasting (HWRF) model: 2015 scientific*
745 *documentation*. Developmental Testbed Center, 113 pp.

746 Wang, C., and S.-K. Lee, 2007: Atlantic warm pool, Caribbean low-level jet, and their
747 potential impact on Atlantic hurricanes. *Geophys. Res. Lett.*, **34**, n/a-n/a.

748 Wang, X., G. Han, Y. Qi, and W. Li, 2011: Impact of barrier layer on typhoon-induced
749 sea surface cooling. *Dynamics of Atmospheres and Oceans*, **52**, 367-385.

750 Wang, Y., and C.-C. Wu, 2004: Current understanding of tropical cyclone structure and
751 intensity changes – a review. *Meteorology and Atmospheric Physics*, **87**, 257-278.

752 Yablonsky, R. M., and I. Ginis, 2009: Limitation of One-Dimensional Ocean Models for
753 Coupled Hurricane–Ocean Model Forecasts. *Mon. Wea. Rev.*, **137**, 4410-4419.

754 Yaremchuk, M., D. Nechaev, and C. Pan, 2011: A Hybrid Background Error Covariance
755 Model for Assimilating Glider Data into a Coastal Ocean Model. *Mon. Wea.*
756 *Rev.*, 139, 1879–1890, doi: 10.1175/2011MWR3510.1.

757 Zhang, W. G., J. L. Wilkin, and H. G. Arango, 2010: Towards an integrated observation
758 and modeling system in the New York Bight using variational methods. Part I:
759 4DVAR data assimilation, *Ocean Modelling*, Volume 35, Issue 3, 119-133, doi:
760 10.1016/j.ocemod.2010.08.003.

761

762

763

764

765

766

767

768

769

770

771 **LIST OF TABLES**

772 Table 1: Observation number assimilated in this study. Observations ranged from March
773 1 to October 13 2014 and were assimilated in the HYCOM model domain covering the
774 North Atlantic.

775

776 Table 2: Data assimilation experiment setup. Details of observations can be found in
777 section 3.2.

778

779 Table 1: Observation number assimilated in this study. Observations ranged from March
 780 1 to October 13 2014 and were assimilated in the HYCOM model domain covering the
 781 North Atlantic.
 782

Obs. Type	Obs. number
Altimetry	1283123
Buoy SST	488011
Shipboard SST	199630
Drifter SST	1360046
Argo floats (profiles)	7562
AXBT (profiles)	1829
Glider (profiles)	180

783
 784

785 Table 2: Data assimilation experiment setup. Details of observations can be found in
 786 section 3.2.

Experiment	Obs assimilated/Remark
NODA	No obs
GLID	Two underwater gliders
CTRL	Standard ocean observations (Jason altimeter, MCSST, AXBT, AXCTD, Argo floats, surface drifters, etc.)
ALL	Gliders+standard ocean observations

787

788 **LIST OF FIGURES**

789

790 Fig. 1: (a) Track and (b) intensity (minimum sea level pressure in hPa and surface
791 maximum wind in knots) of Hurricane Gonzalo (2014).

792 Fig. 2: (a) Location of underwater glider profile observations sampled north of Puerto
793 Rico during July-November 2014 (red dots). During October 8-13, 2014, the glider
794 travelled along section AB, sampling temperature and salinity conditions before the
795 passage of Hurricane Gonzalo (black line). Pre-storm (b) temperature and (c) salinity
796 conditions between sites A and B. Initial (d) temperature and (e) salinity profiles at site B
797 on October 13, 2014, before the passage of Hurricane Gonzalo.

798 Fig. 3: (a) Latitude-time Hovmoller diagram for monthly sea height anomaly residuals
799 (seasonal cycle removed) during 1993-2015 along section AB. (b) Time-series of TCHP
800 residuals at site B during 1993-2015.

801 Fig. 4: Standard ocean observation distribution from September 29 to October 13.

802 Fig. 5: (a) Temperature and (b) salinity profiles at 0000 UTC October 13 2014 from four
803 experiments, compared to the glider observation.

804 Fig. 6: Temperature (in $^{\circ}\text{C}$; a-d) and salinity (e-h) errors profile of four experiments
805 (model-obs) at 0000 UTC October 13 2014.

806 Fig. 7: Same as Fig. 5 but for (a) density and (b) buoyancy frequency profiles.

807 Fig. 8: SST (left panel) and TCHP (right panel) of NODA (b and f), GLID (c and g) and
808 CTRL (d and h), along with the observation (a and e) at 0000 UTC October 13,
809 overlapped with the best track (a and e) or the predicted track of each individual

810 experiment (b-d, f-h). 28.5 °C and 26 °C isotherms are highlighted in SST plots (a-d). 60
811 and 80 kJcm⁻² contours are highlighted in TCHP plots (e-h). The blue lines in (a) and (e)
812 denote the locations of two underwater gliders deployed in 2014.

813 Fig. 9: SST of four experiments and remote sensing observations at 0000 UTC October
814 13 2014, averaged along best track (for observation) and the predicted future tracks (for
815 four experiments) within 84 km radius from the storm centers. The dashed line denotes
816 the track location where is closest to the glider at 0000 UTC October 13 2014.

817 Fig. 10: Ocean temperature errors of NODA (a), GLID (b), CTRL (c) and ALL (d) with
818 depth during 0000 UTC October 13 to 0000 UTC October 15 at 66° W, 20.2° N.

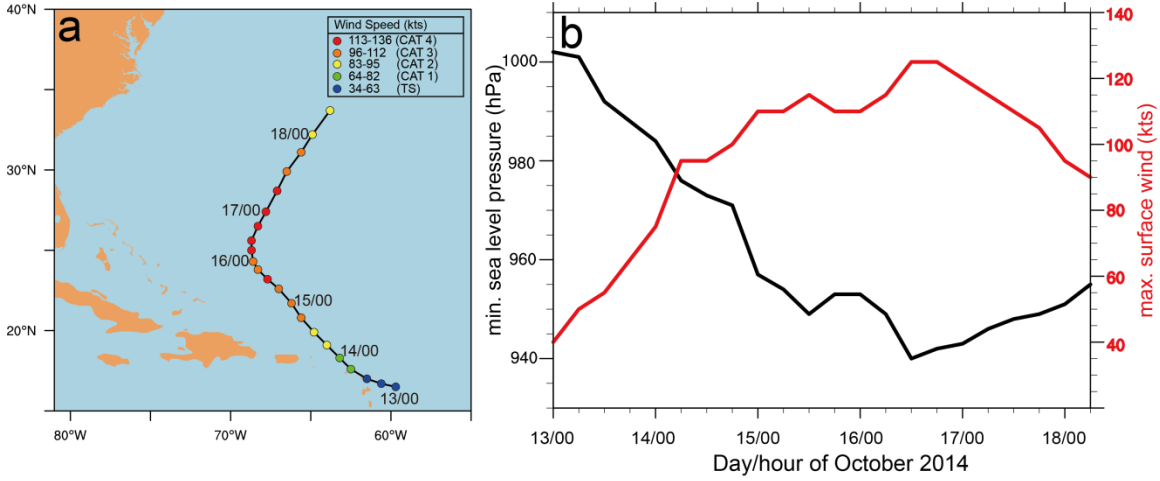
819 Fig. 11: Same as Fig. 10 but for salinity errors.

820 Fig. 12: Hurricane Gonzalo track forecast (a), minimum sea level pressure (center
821 pressure) (b) and maximum wind forecasts (c), along with the best track. The dashed line
822 in b and c is the same as Fig. 9.

823

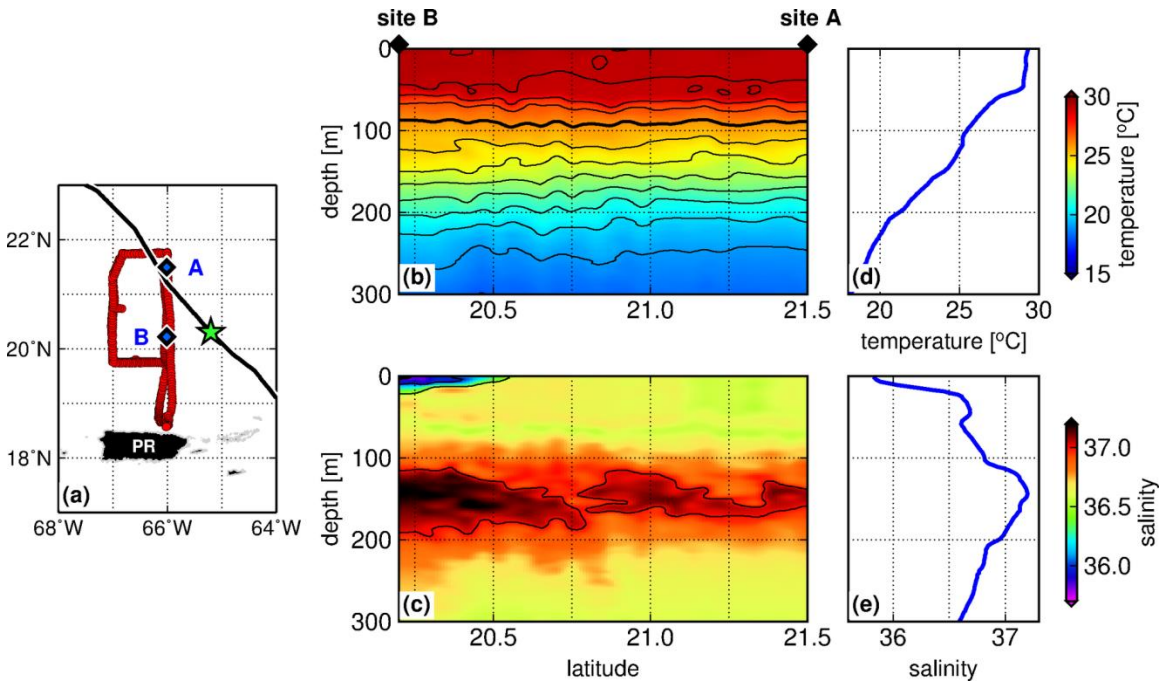
824
825
826
827
828
829
830
831

832
833



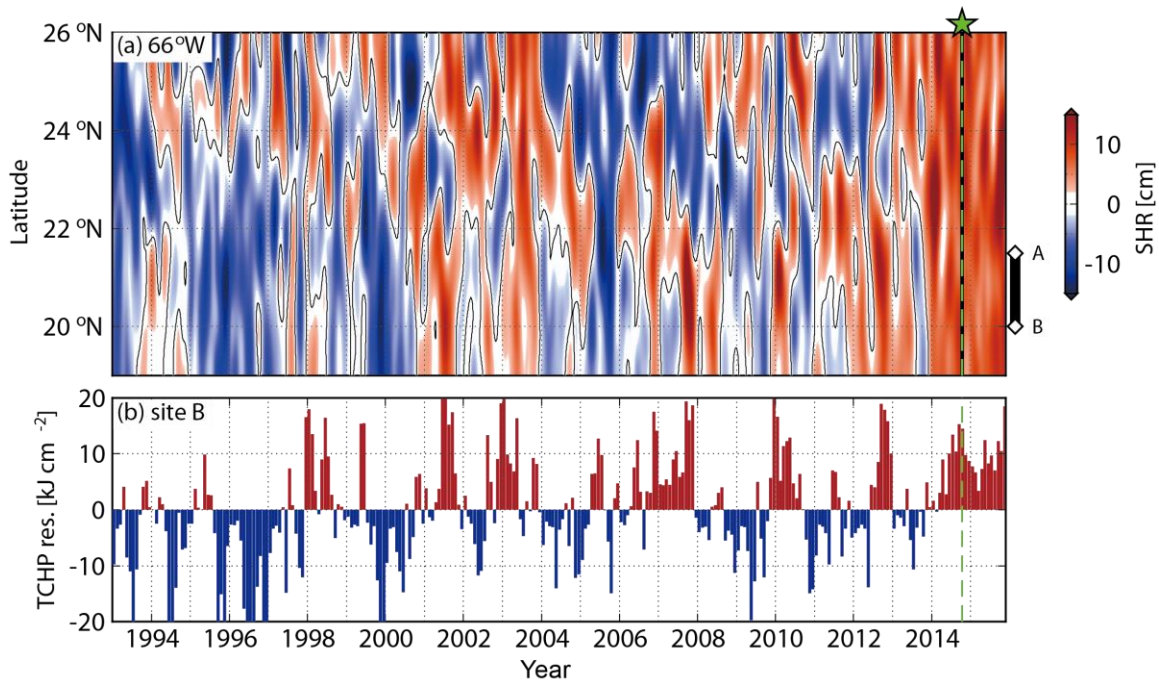
834
835
836
837
838
839
840

Fig. 1: (a) Track and (b) intensity (minimum sea level pressure in hPa and surface maximum wind in knots) of Hurricane Gonzalo (2014).



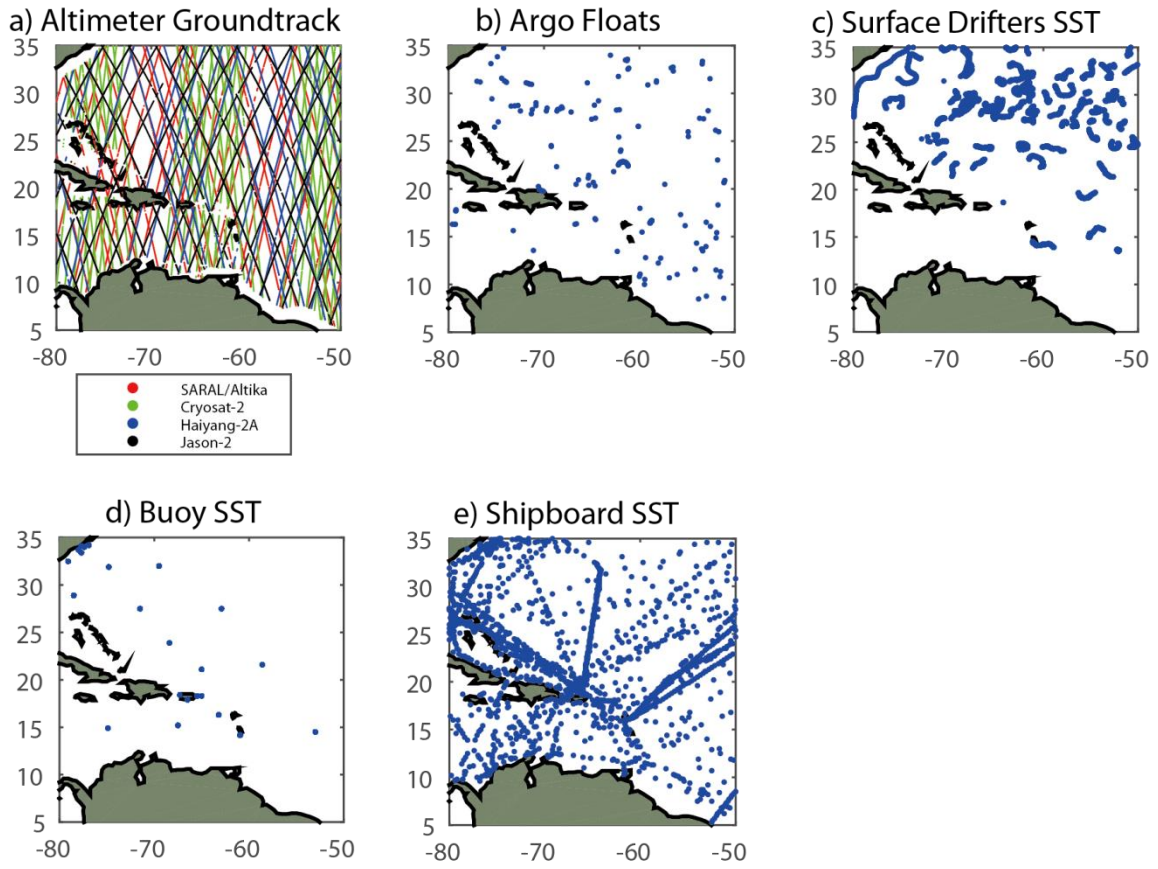
841
842

843 Fig. 2: (a) Location of underwater glider profile observations sampled north of Puerto
 844 Rico during July-November 2014 (red dots). During October 8-13, 2014, the glider
 845 travelled along section AB, sampling temperature and salinity conditions before the
 846 passage of Hurricane Gonzalo (black line). Pre-storm (b) temperature and (c) salinity
 847 conditions between sites A and B. Initial (d) temperature and (e) salinity profiles at site B
 848 on October 13, 2014, before the passage of Hurricane Gonzalo.



849
 850
 851 Fig. 3: (a) Latitude-time Hovmoller diagram for monthly sea height anomaly residuals
 852 (seasonal cycle removed) during 1993-2015 along section AB. (b) Time-series of TCHP
 853 residuals at site B during 1993-2015.

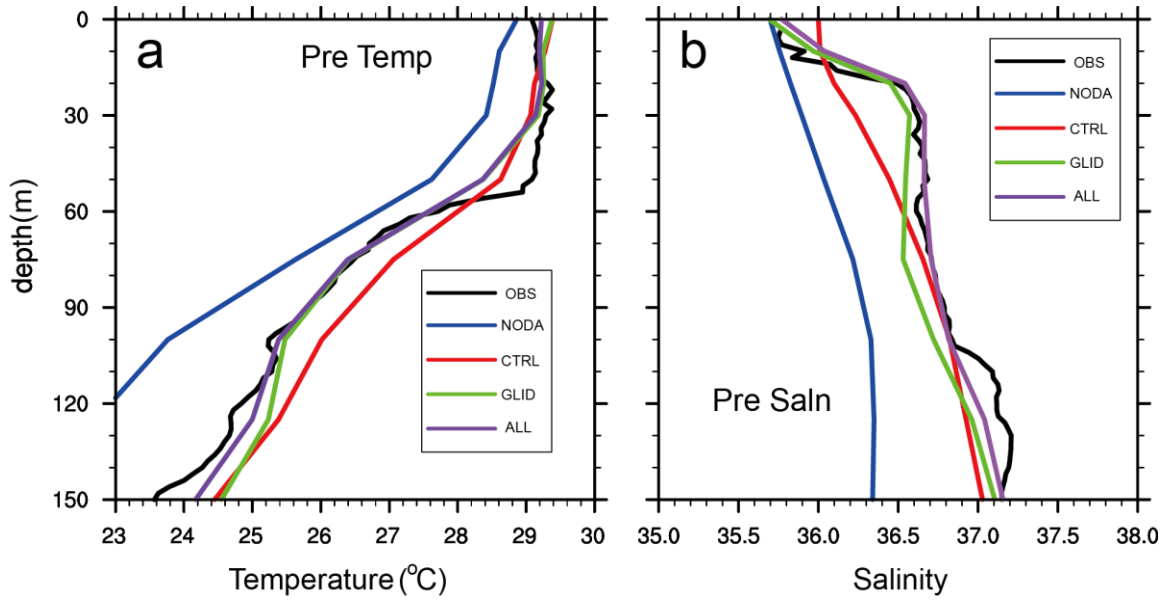
854



855
856

857 Fig. 4: Standard ocean observation distribution from September 29 to October 13.

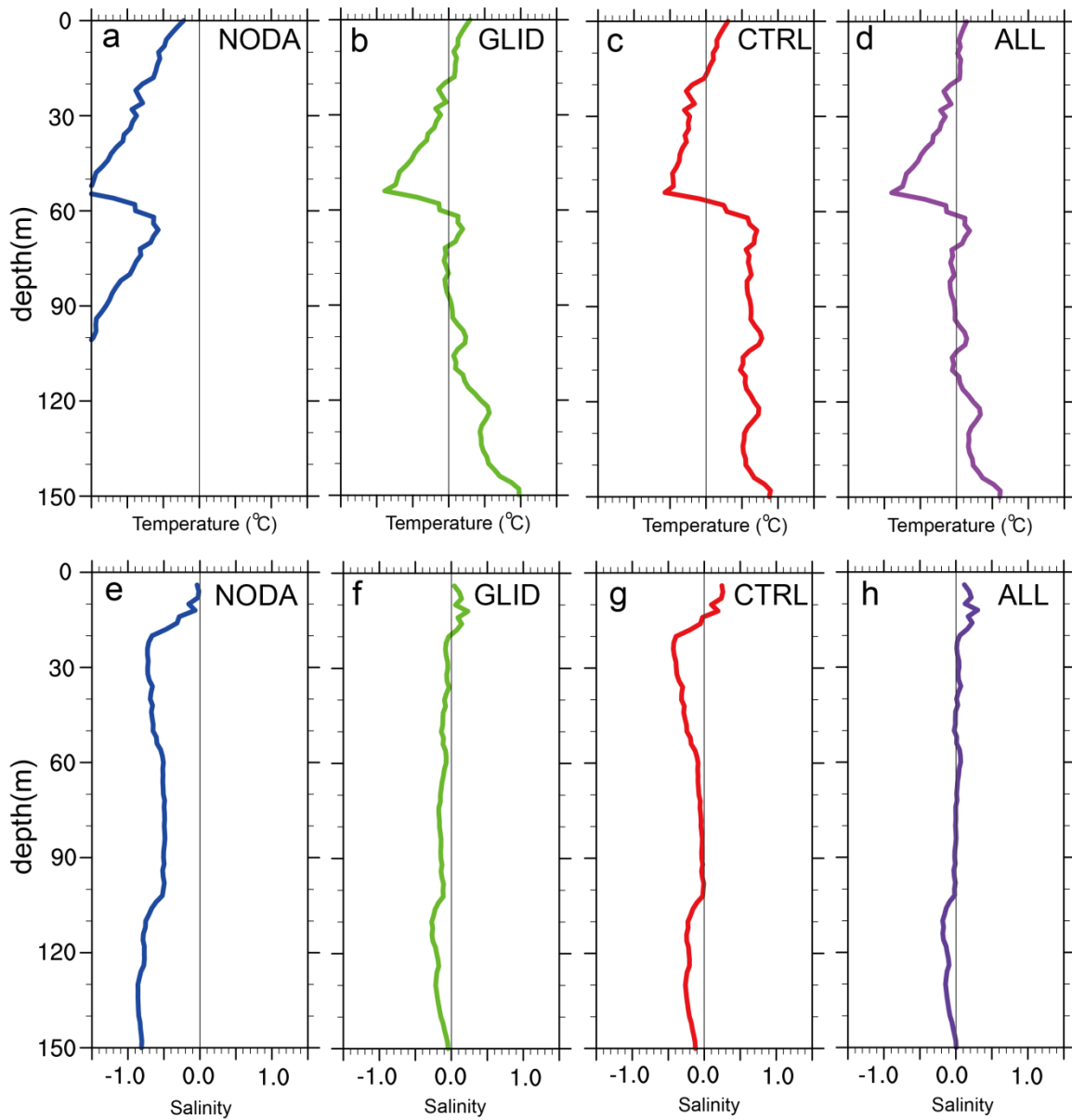
858
859
860
861
862



863
864

865 Fig. 5: (a) Temperature and (b) salinity profiles at 0000 UTC October 13 2014 from four
866 experiments, compared to the glider observation.

867
868
869
870

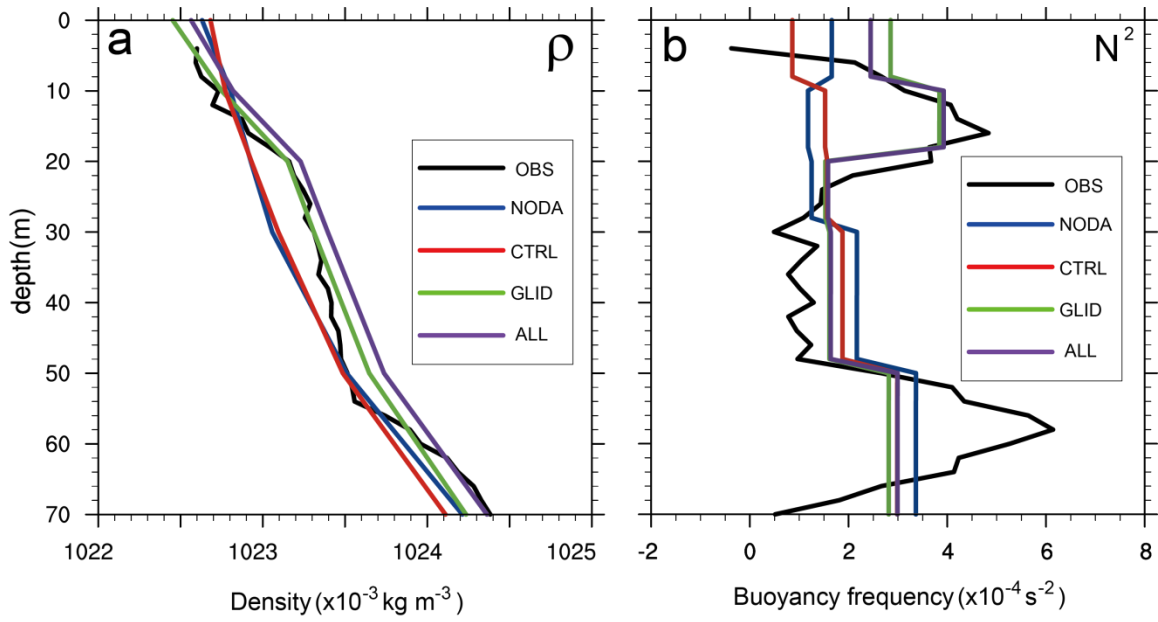


871
872

873 Fig. 6: Temperature (in $^{\circ}\text{C}$; a-d) and salinity (e-h) errors profile of four experiments

874 (model-obs) at 0000 UTC October 13 2014.

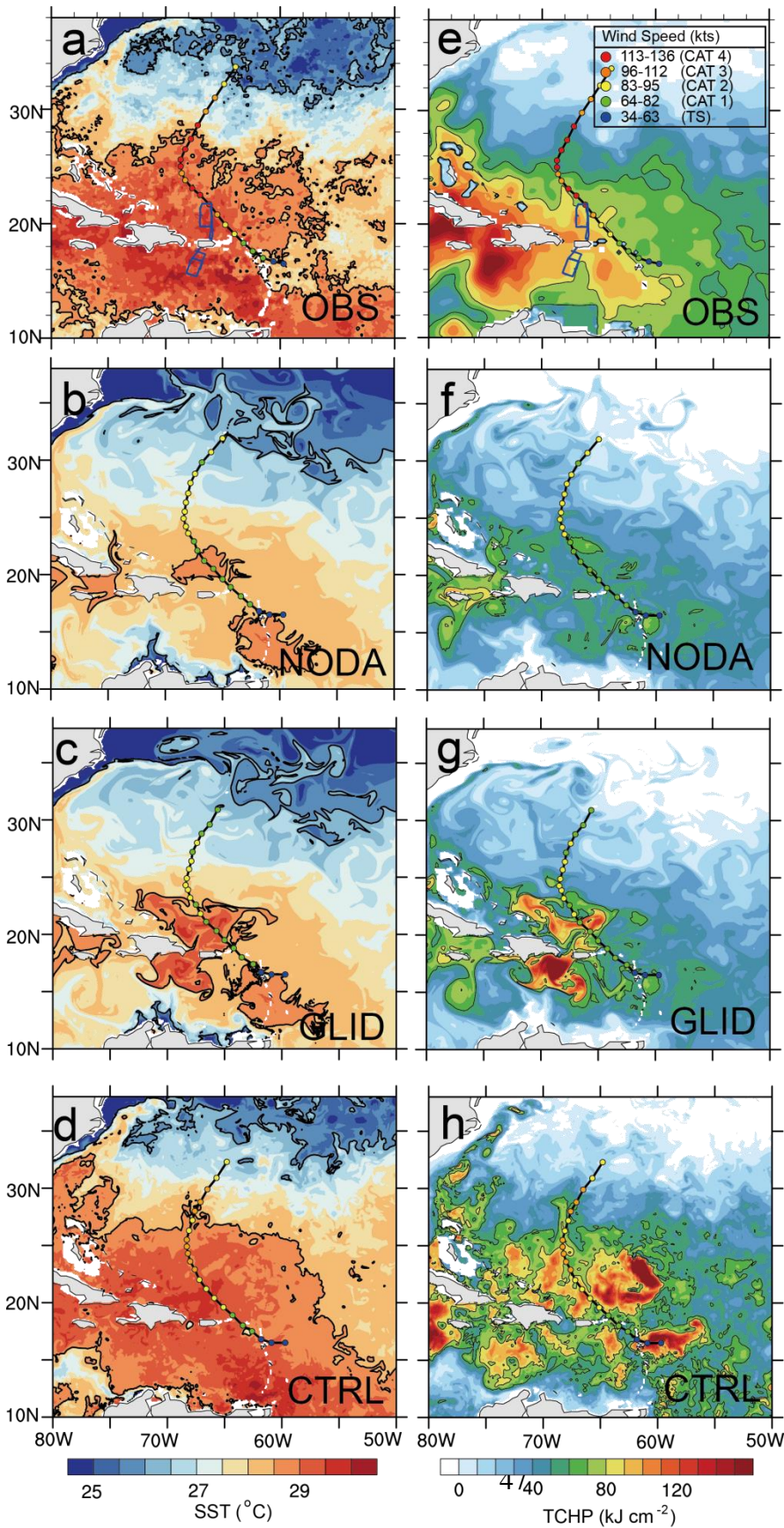
875



876
877

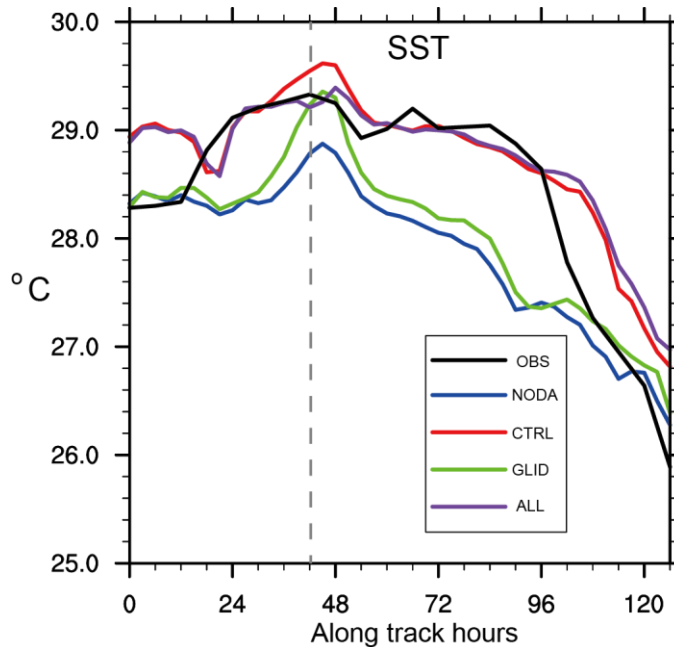
878 Fig. 7: Same as Fig. 5 but for (a) density and (b) buoyancy frequency profiles.

879
880
881

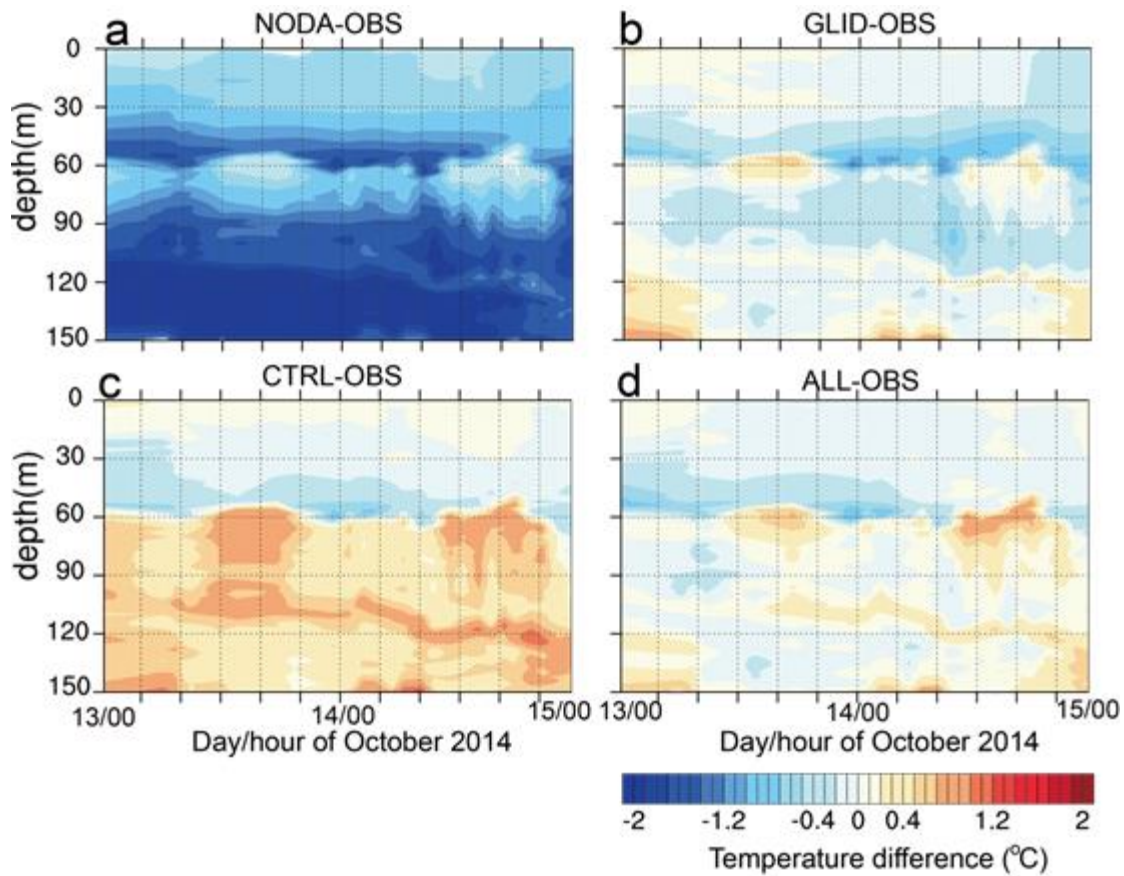


883 Fig. 8: SST (left panel) and TCHP (right panel) of NODA (b and f), GLID (c and g) and
 884 CTRL (d and h), along with the observation (a and e) at 0000 UTC October 13,
 885 overlapped with the best track (a and e) or the predicted track of each individual
 886 experiment (b-d, f-h). 28.5 °C and 26 °C isotherms are highlighted in SST plots (a-d). 60
 887 and 80 kJcm⁻² contours are highlighted in TCHP plots (e-h). The blue lines in (a) and (e)
 888 denote the locations of two underwater gliders deployed in 2014.

889
 890

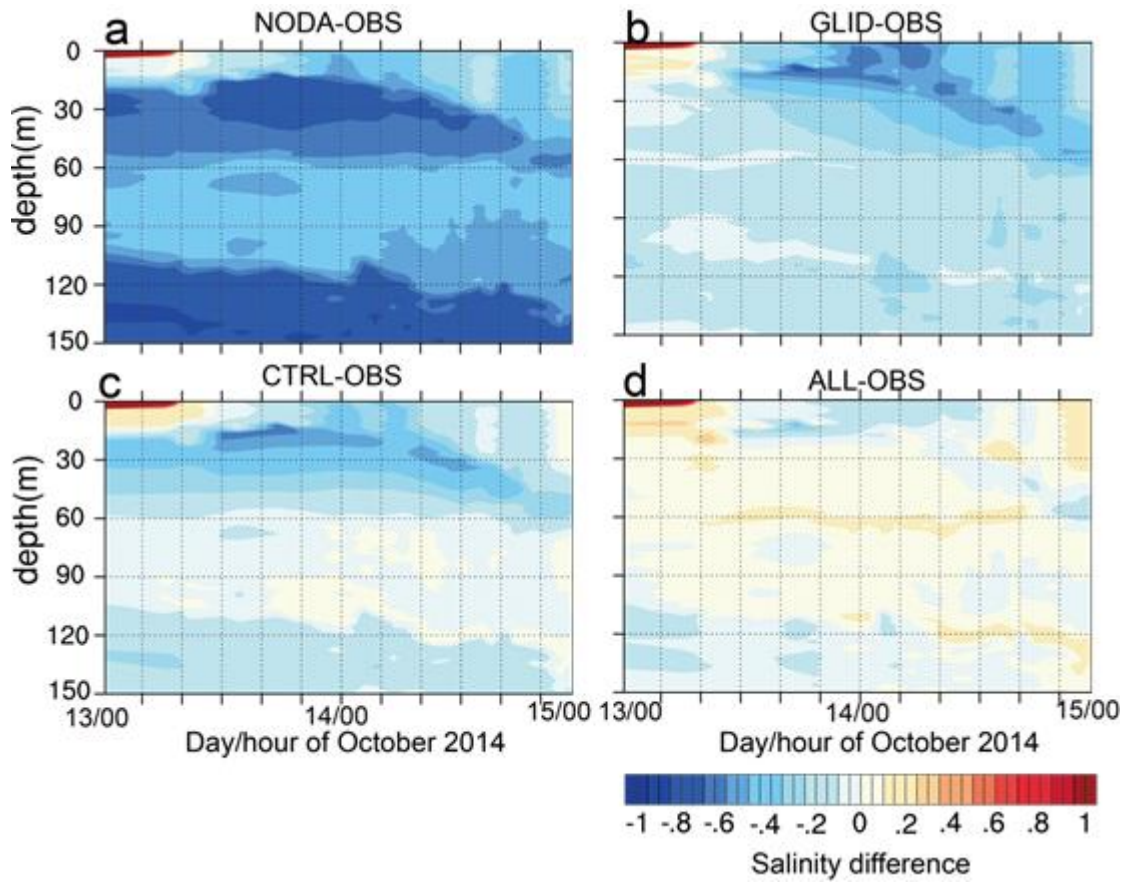


891
 892 Fig. 9: SST of four experiments and remote sensing observations at 0000 UTC October
 893 13 2014, averaged along best track (for observation) and the predicted future tracks (for
 894 four experiments) within 84 km radius from the storm centers. The dashed line denotes
 895 the track location where is closest to the glider at 0000 UTC October 13 2014.



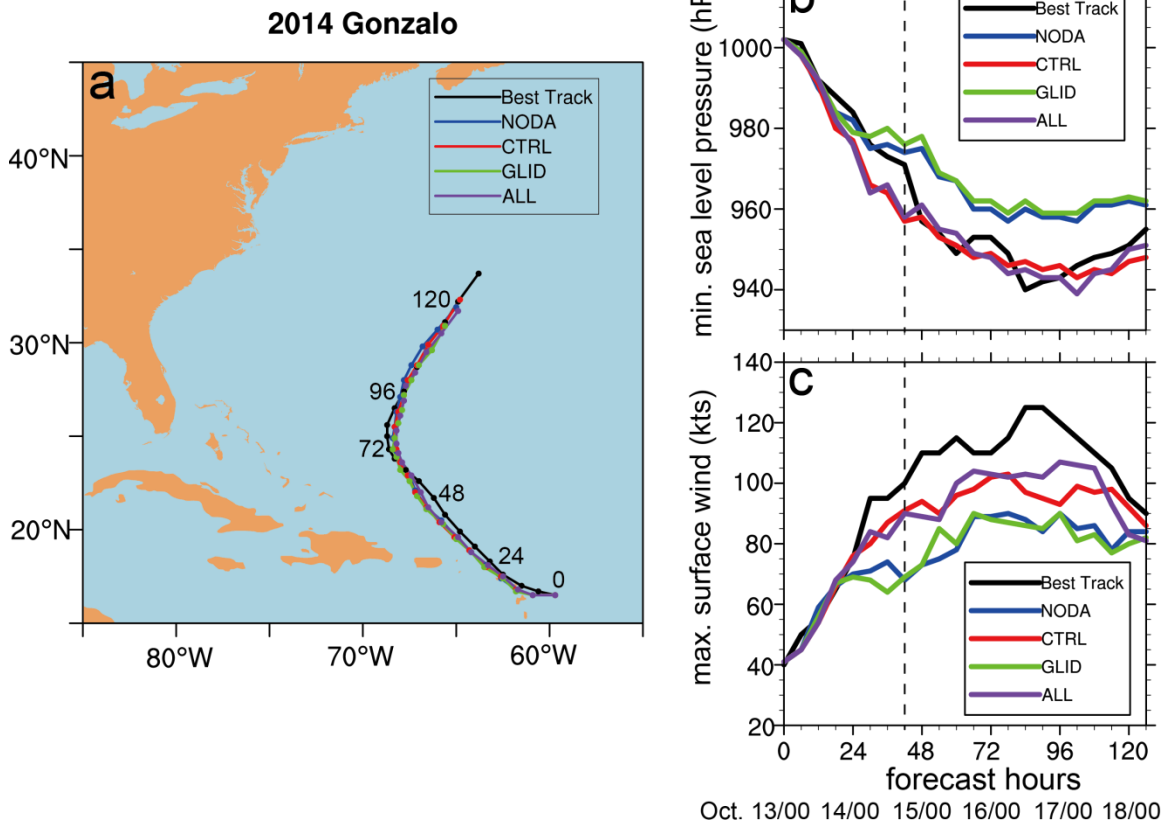
896
897

898 Fig. 10: Ocean temperature errors of NODA (a), GLID (b), CTRL (c) and ALL (d) with
899 depth during 0000 UTC October 13 to 0000 UTC October 15 at 66° W, 20.2° N.



900 Fig. 11: Same as Fig. 10 but for salinity errors.
 901

902



903
 904 Fig. 12: Hurricane Gonzalo track forecast (a), minimum sea level pressure (center
 905 pressure) (b) and maximum wind forecasts (c), along with the best track. The dashed line
 906 in b and c is the same as Fig. 9.